Opto-Electronic Advances

Original Article

2018, Vol. 1, No. 8

DOI: 10.29026/oea.2018.180014

Enhancement of laser ablation via interacting spatial double-pulse effect

Rui Zhou[1]*, Shengdong Lin[1], Ye Ding[2,3], Huan Yang[2,4], Kenny Ong Yong Keng[2] and Minghui Hong[2]*

A novel spatial double-pulse laser ablation scheme is investigated to enhance the processing quality and efficiency for nanosecond laser ablation of silicon substrate. During the double-pulse laser ablation, two splitted laser beams simultaneously irradiate on silicon surface at a tunable gap. The ablation quality and efficiency are evaluated by both scanning electron microscope and laser scanning confocal microscope. As tuning the gap distance, the ablation can be significantly enhanced if the spatial interaction between the two splitted laser pulses is optimized. The underlying physical mechanism for the interacting spatial double-pulse enhancement effect is attributed to the redistribution of the integrated energy field, corresponding to the temperature field. This new method has great potential applications in laser micromachining of functional devices at higher processing quality and faster speed.

Keywords: double-pulse; laser ablation; efficiency; quality

Zhou R, Lin S D, Ding Y, Yang H, Ong Y K K *et al*. Enhancement of laser ablation via interacting spatial double-pulse effect. *Opto-Electronic Advances* **1**, 180014 (2018).

Introduction

Short pulsed laser has been employed as an effective tool for micromaching. Versatile methods are offered for cutting, drilling and modification of various engineering materials[1–3]. Compared to other fabrication technologies, such as chemical wet etching and electrical erosion[4,5], laser micromaching has particular benefits due to non-contact processing with high accuracy, repeatability and flexibility[6–9]. Therefore, laser has become a powerful tool as an excellent alternative to the conventional microprocessing methods[10,11]. However, the speed of laser processing is still far from an economical industrial use[12]. As thermal diffusion dominates the nanosecond laser ablation, the ablation efficiency is restricted by the ablation threshold of materials, which strongly depends on their physical properties, such as absorption coefficient, thermal diffusivity, melting and boiling behaviors[13,14].

A series of research has been conducted to develop feasible approaches in order to enhance the laser ablation quality and efficiency. A common method is to coat the substrate material surface with a layer of energy absorbing material, such as graphite powder, mica or black paint[15]. The coating materials strongly enhance the absorption of the laser energy by converting the optical energy into thermal energy, which is transferred to the substrate materials to enhance the laser micromachining. A hybrid laser-coaxial argon plasma ablation also provides an effective route to increase volume ablation efficiency compared to the conventional laser ablation[16], which is attributed to the de-excitation of argon plasma species and the accompanying energy deposition at the generated debris and substrate surface. It is also found that another phenomenon existing in the plasma assisted laser ablation is the formation of micro-bubbles and holes on substrate surfaces[17]. It can reduce the optical reflectivity and modify thermo-physical properties of the processed substrate surface, further decreasing the laser-ablated threshold fluence. Temporal double-pulse laser ablation is also a common method[18] by the first laser pulse to modify the properties of substrate material, leading to the enhanced laser ablation of the subsequent laser pulses. However,

[1]Department of Mechanical and Electrical Engineering, School of Aerospace Engineering, Xiamen University, Xiamen 361102, China; [2]Department of Electrical and Computer Engineering, National University of Singapore, Singapore 117576; [3]School of Mechatronics Engineering, Harbin Institute of Technology, Harbin 150001, China; [4]College of Mechanical and Electrical Engineering, Wenzhou University, Wenzhou, 325035, China

* Correspondence: R Zhou, E-mail: rzhou2@xmu.edu.cn; M H Hong, E-mail: elehmh@nus.edu.sg

Received 13 August 2018; accepted 3 September 2018; accepted article preview online 30 September 2018

most of the developed technologies need to be supplemented by complicated system setups. Extra surface modifications and defects caused by these methods, which are disadvantageous to the practical applications, is also inevitable and uncontrollable.

In this paper, a spatial double-pulse laser ablation system is proposed and studied to increase the laser ablation efficiency and quality. Two splitted laser pulses are irradiated on the surface of the material at the same time at a tunable spatial gap between the double laser spots. By the interaction of the splitted laser pulses, the laser energy distribution of substrate surface can be modified, resulting in the change of temperature field to enhance the laser ablation efficiency. The understanding of the spatial double-pulse enhancement effect in the micromachining process significantly broadens the practical applications.

Experimental

Figure 1 shows a schematic diagram of the experimental setup for the spatial double-pulse laser ablation, which includes a nanosecond fiber laser, two polarization beam splitters (PBS1 and PBS2), three mirrors (M1–M3), a focal lens (FL) and a linear motion stage. The nanosecond pulsed fiber laser is operated at 1064 nm with a pulse duration of ~100 ns in this study. The repetition rate, laser power and laser fluence are 70 kHz, 10 W and 3.71 J/cm^2, respectively. A linear polarized laser beam emitted from the fiber laser passes through the first beam splitter (PBS1), and then is divided into two splitted laser beams (LB1 and LB2) with the equal power, which travel along respective directions. After being reflected by two mirrors, the splitted laser beams converge in the second beam splitter (PBS2), then are reflected by the third mirror. The reflected laser beams are delivered and focused by a focal lens onto the surface of silicon substrate, which is put on a linear motion stage with a spatial resolution of 2 μm. The focal length of the lens is 100 mm. The laser beam has a Gaussian distribution of spatial intensity and the laser spot diameter on the silicon surface is around 70 μm. The motion stage and the laser are controlled by a computer. A polished single-crystal undoped silicon wafer with a thickness of 525±25 μm is used as samples. The gap between the two focused laser spots ranges from 60 to 100 μm at an interval of 20 μm, adjusted by controlling the angle of M2. Craters and grooves are both measured to analyze the laser ablation enhancement effect. Laser scanning confocal microscope (OLYMPUS, OSL 4100) and scanning electron microscope are employed to characterize the surface morphology, 2D profiles and 3D reconstructions. The ablation volume (V) of the crater is estimated by considering both the cross-sectional area (S) from the point of side-view and the diameter (D) of the crater rim. S is obtained from the 2D profile curve and then V is calculated from multiplying S by (ΠD/4).

Results and discussion

Figure 2 shows the laser ablated craters on silicon surface. Craters are fabricated by tuning the spatial gap between two splitted laser beams. As illustrated in Fig. 2(a), for the gap at 100 μm, two relatively independent craters with narrow crater rims could be distinguished by double-pulse laser ablation. SEM image indicates that the diameters of the craters are about 70 μm. It is observed that the bottom of the craters and the area between them are uneven with a large amount of deposited debris. During the laser ablation, the dynamics of the materials' ejection and nucleation are two dominant factors for the formation of craters. Nanosecond laser can heat, melt and evaporate the substrate materials, inducing the materials' breakdown and then to be ejected from the crater. After the laser irradiation, the melted and evaporated materials in the crater resolidified, causing the bottom to be rough with protrusions[19]. The higher laser fluence generates more protrusions. Meanwhile, the ejected materials de-

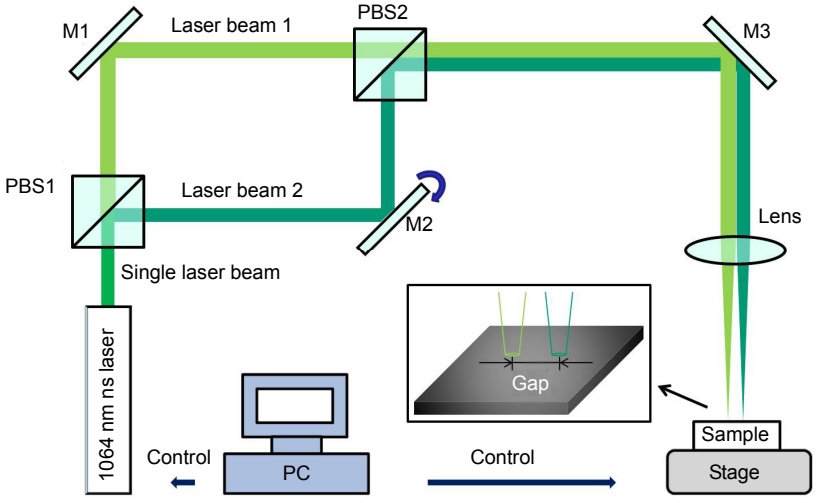

Fig. 1 | Schematic diagram of the experimental setup for the spatial double-pulse laser ablation.

posited around the crater, leading to the formation of debris between the craters. It is roughly calculated for total laser ablation volume at 4.28×10^4 μm^3 for the craters in Fig. 2(a).

While decreasing the gap distance of two splitted laser beams to 80 μm as shown in Fig. 2(b), the 3D reconstruction and 2D profile of the crater clearly indicate that the side-by-side circular craters in Fig. 2(a) are merged into a single gourd-shaped crater and the material between the two craters is completely removed, leaving a broad flat bottom in the width more than 100 μm with only a few protrusions, indicating the improved quality of laser ablation. In addition, it is also observed that the edge height is increased by a larger amount of debris piled up in the region surrounding the crater, leading to a broader width of crater rim. In consideration of the diameters of independent craters at about 70 μm in Fig. 2(a), it is interestingly found that the ablation volume of the gourd-shaped crater is approximately 7.05×10^4 μm^3 in Fig. 2(b) at the same total laser power of 10 W, which is significantly increased by 65%. Obviously, the laser ablation rate is greatly enhanced by significantly increased depth and side-view cross-sectional area of the crater. When the gap of double-pulse beams is reduced, their ablation areas overlap with each other. The reason for the complete removal of materials between the double pulse laser spots is mainly related to the change of temperature field due to the redistribution of laser energy while tuning the gap of double-pulse beams.

Furthermore, as the gap continues decreasing to 60 μm in Fig. 2(c), the enhancement is less significant than that at 80 μm, although the similar gourd-shape crater is also obtained. The projected area of the crater in Fig. 2(c) with an estimated ablation volume at 4.20×10^4 μm^3 is almost

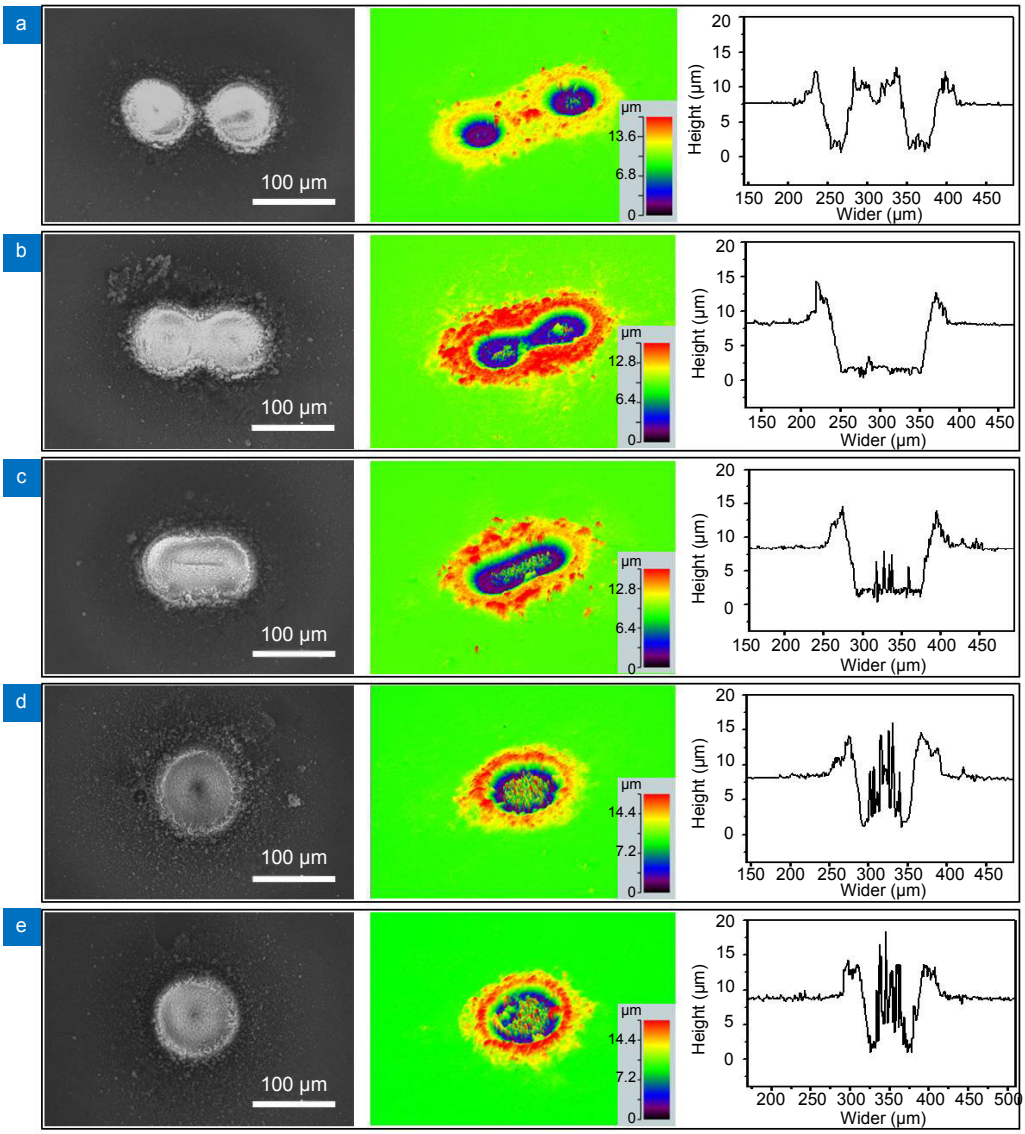

Fig. 2 | SEM images, 3D reconstructions and 2D profiles of craters created by the splitted double-pulse laser beams at different gaps of (a) 100 μm, (b) 80 μm, (c) 60 μm, (d) 0 μm, and (e) by single laser beam at a total laser power of 10 W.

the same as the total ablation volume of the double laser beams in Fig. 2(a). At the same time, it is observed that a large number of protrusions appear at the bottom with a reduced edge height of debris on the crater rim due to the higher laser fluence and broader crater opening, respectively. As the gap continuously decreasing to 0 μm in Fig. 2(d), the number and volume of protrusions at the bottom of craters obviously increase due to the significantly enhanced laser energy by completely overlapping of the double-pulse beams. It could be seen that the heights of some protrusions are even larger than the depth of the crater with decreased ablation volume at 1.24×10^4 μm^3. In this case, the laser micromaching is unable to produce a desired crater. The result is almost the same as that of single beam laser processing with an ablation volume at 1.15×10^4 μm^3 in Fig. 2(e) at the same total laser power of 10 W. Therefore, it can be concluded that the gap around 80 μm shows the optimal performance in laser ablation efficiency and quality.

To further understand the observed interesting phenomena and reveal the underlying physical mechanism for the interacting spatial double-pulse enhancement effect, the double-pulse laser system is employed to fabricate grooves. In the experiment, two intersecting straight grooves can straightforwardly reflect the effect of gap distance as shown in Fig. 3. Three different areas being fabricated are illustrated in Fig. 3(a). In each area, the morphology and groove depth of substrate are gradually changed with gap. In Area I, the gap is larger than 100 μm for the two splitted laser beams. The laser micromaching is unable to produce obvious groove due to low laser fluence. In this area, there exist a number of tiny particles in the size of hundreds of nanometers along the two straight grooves. In Area II, the gap decreases from >100 μm to >50 μm, and the double-pulse laser spots begin to interact. It is observed that a group of nanoparticles in a higher density are accumulated on the edges of grooves due to the redistribution of laser energy from the overlapping of double pulses. The interacting effect of double-pulse beams results in the redistribution of temperature profile in this area, leading to the material evaporation in the intersecting central part of grooves. Then the vaporized material condensates into particles via strong collisions with ambient gas molecules, finally scattering around this area. In this case, the evaporated material can be ejected further away from the laser scanning area by piling up on the edge of grooves. Hence, the density of nanoparticles along the edge of grooves is obviously increased and the depth of the grooves also increases with the appearance of some protrusions resulted from the moving melted pool of substrate surface by laser ablation. Furthermore, Fig. 3(b) shows there exist more protrusions in the groove center of Area III at the gap < 50 μm with higher density of nanoparticles piled up on the groove edges. In Area III, more substrate materials are melted with enhanced material evaporation simultaneously, where the number and volume of protrusions at the bottom of the grooves significantly increase due to the enhanced laser energy by completely overlapping of double-pulse beams. In supplementary materials, the effect of double-pulse laser is further studied by processing parallel grooves.

Above studies illustrate that the gap strongly affects the double pulse laser ablation due to the spatial interaction of two splitted laser beams. Compared with laser ablation by single laser beam at the same total power, the interacting spatial double-pulse laser ablation shows optimized ablation efficiency in a suitable gap. The main mechanism behind is attributed to the redistribution of temperature field. As it can be seen in Fig. 4, the change of temperature field distributions with different gaps is modeled to reveal the physical mechanism. Three types of regions, including regions I, II and III, are described for all models along the axial direction of substrate surfaces. In regions II and III, the substrate surface could be melted and formed liquid pools. In this process, the protrusions are generated on the surfaces of liquid pools. However, the heating temperature is not high enough to vaporize the substrate materials in region II. Material evaporation only happens in region III, where part of the evaporated materials could be resolidified and accumulate on the edge of the craters in region II. In Fig. 4(a), when two splitted

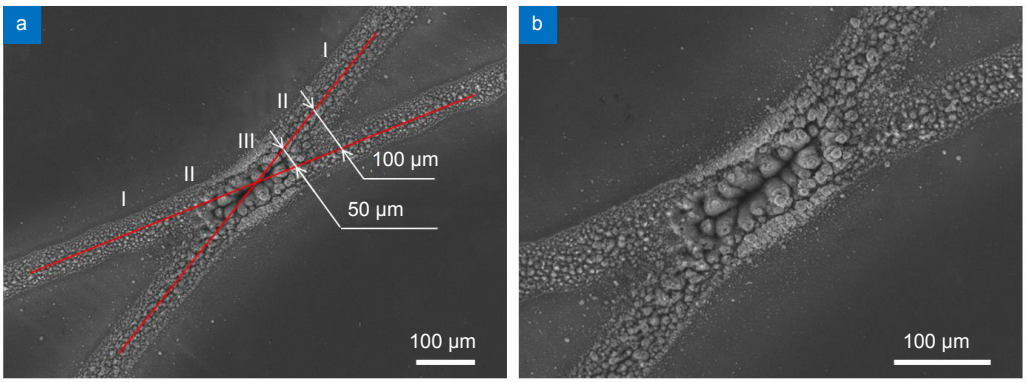

Fig. 3 | SEM images of (a) two intersecting grooves processed by double laser pulses and (b) zoom-in state.

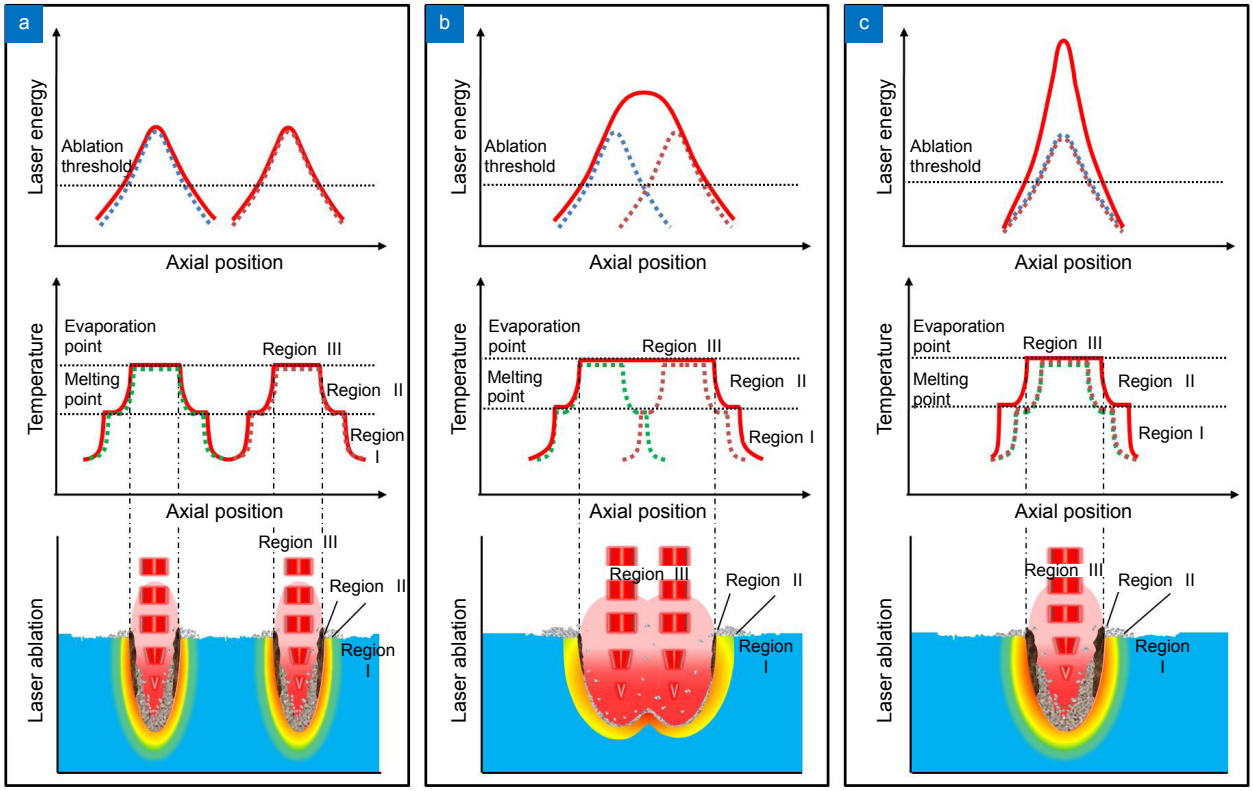

Fig. 4 | The schematic diagram of distributions of energy field (upper), temperature field (middle) and the interaction between laser and silicon (bottom) at different gaps. (**a**) Large gap. (**b**) Optimal gap. (**c**) Zero gap.

laser beams irradiate on the target with a large gap, there is no interaction between them with independent distributions of temperature fields. Hence, the central temperature between the two splitted laser pulses is insufficient to evaporate the silicon material surface due to relatively low laser energy. Therefore, there are only two ablation craters on the substrate material surface. However, as the gap decreases to a sufficiently small distance, the integrated distribution of temperature field begins to change by overlapping with each other. While the gap decreases to an optimized level, the energy fields of two laser pulses could interact with each other, resulting in an integrated temperature field as demonstrated in Fig. 4(b). It indicates the temperature of the area between the two laser pulses can be risen up to the evaporation point in corresponding to region III. During the laser ablation, silicon materials can be heated, melted, and eventually evaporated. The evaporated material could be removed quickly from the processing area, resulting in an obvious crater with broader width and larger depth. It means that the efficiency of laser ablation could be enhanced by optimizing the integrated temperature field on substrate surface. Meanwhile, for spatial double-pulse laser ablation, the laser ablated craters are larger and the channels are wider with an optimized setup. If the gap is smaller than the optimized gap for the laser ablation, the efficiency of laser ablation begins to decrease. Figure 4(c) shows the distribution of temperature field for double pulse laser without gap or single laser at the same total laser power. In this case, although the materials also can be evaporated due to the high temperature of surface, the laser ablation area decreases with narrower width of temperature field distribution, leading to fewer removed substrate materials. Additionally, since the central temperature of the laser ablation area is relatively high, it can induce a larger number of protrusions at the bottom as shown in Figs. 2(d) and 2(e), which reduces the ablation quality. Hence, only the suitable gap can achieve the highest ablation efficiency and best ablation quality.

Conclusions

In this work, a spatial double-pulse laser ablation system is designed to increase the laser ablation quality and efficiency on silicon substrate. During the double-pulse laser ablation, the laser ablation quality and efficiency could be enhanced as the gap distance is optimized at about 80 μm. The enhancement of laser ablation in optimized gaps is possibly resulted from spatial interacting of splitted double pulses, leading to the redistribution of temperature field, corresponding to the integrated energy field. Experimental analysis shows that the ablation efficiency could be enhanced by 65% with better quality of micromaching by the interacting spatial double-pulse enhancement effect.

References

1. Choudhury I A, Shirley S. Laser cutting of polymeric materials: an experimental investigation. *Opt Laser Technol* **42**, 503–508 (2010).
2. Ancona A, Döring S, Jauregui C, Röser F, Limpert J *et al*. Femtosecond and picosecond laser drilling of metals at high repetition rates and average powers. *Opt Lett* **34**, 3304–3306 (2009).
3. Miyamoto I, Cvecek K, Okamoto Y, Schmidt M. Internal modification of glass by ultrashort laser pulse and its application to microwelding. *Appl Phys A* **114**, 187–208 (2014).
4. Lee Y J, Kuo H C, Lu T C, Wang S C, Ng K W *et al*. Study of GaN-based light-emitting diodes grown on chemical wet-etching-patterned sapphire substrate with V-shaped pits roughening surfaces. *J Lightwave Technol* **26**, 1455–1463 (2008).
5. Hyypio D. Mitigation of bearing electro-erosion of inverter-fed motors through passive common-mode voltage suppression. *IEEE Trans Ind Appl* **41**, 576–583 (2005).
6. Meng H Y, Liao J H, Zhou Y H, Zhang Q M. Laser micro-processing of cardiovascular stent with fiber laser cutting system. *Opt Laser Technol* **41**, 300–302 (2009).
7. Watanabe W, Li Y, Itoh K. Ultrafast laser micro-processing of transparent material. *Opt Laser Technol* **78**, 52–61 (2016).
8. Rizvi N H, Apte P. Developments in laser micro-machining techniques. *J Mater Process Technol* **127**, 206–210 (2002).
9. Lu B H, Lan H B, Liu H Z. Additive manufacturing frontier: 3D printing electronics. *Opto-Electron Adv* **1**, 170004 (2018).
10. Xu K C, Zhang C T, Zhou R, Ji R, Hong M H. Hybrid micro/nano-structure formation by angular laser texturing of Si surface for surface enhanced Raman scattering. *Opt Express* **24**, 10352–10358 (2016).
11. Mahdieh M H, Nikbakht M, Eghlimi Moghadam Z, Sobhani M. Crater geometry characterization of Al targets irradiated by single pulse and pulse trains of Nd:YAG laser in ambient air and water. *Appl Surf Sci* **256**, 1778–1783 (2010).
12. König J, Nolte S, Tünnermann A. Plasma evolution during metal ablation with ultrashort laser pulses. *Opt Express* **13**, 10597–10607 (2005).
13. Crawford T H R, Borowiec A, Haugen H K. Femtosecond laser micromachining of grooves in silicon with 800 nm pulses. *Appl Phys A* **80**, 1717–1724 (2005).
14. Bulgakova N M, Bulgakov A V. Pulsed laser ablation of solids: transition from normal vaporization to phase explosion. *Appl Phys A* **73**, 199–208 (2001).
15. Zhou M, Zhang Y K, Cai L. Laser shock forming on coated metal sheets characterized by ultrahigh-strain-rate plastic deformation. *J Appl Phys* **91**, 5501–5503 (2002).
16. Gerhard C, Roux S, Brückner S, Wieneke S, Viöl W. Atmospheric pressure argon plasma-assisted enhancement of laser ablation of aluminum. *Appl Phys A* **108**, 107–112 (2012).
17. Kajita S, Ohno N, Takamura S, Sakaguchi W, Nishijima D. Plasma-assisted laser ablation of tungsten: reduction in ablation power threshold due to bursting of holes/bubbles. *Appl Phys Lett* **91**, 261501 (2007).
18. Babushok V I, DeLucia Jr F C, Gottfried J L, Munson C A, Miziolek A W. Double pulse laser ablation and plasma: laser induced breakdown spectroscopy signal enhancement. *Spectrochim Acta Part B: At Spectrosc* **61**, 999–1014 (2006).
19. Jansen E D, Asshauer T, Frenz M, Motamedi M, Delacrétaz G *et al*. Effect of pulse duration on bubble formation and laser - induced pressure waves during holmium laser ablation. *Lasers Surg Med* **18**, 278–293 (1996).

Acknowledgements

We are grateful for financial supports from the National Natural Science Foundation of China under Grant (No. 61605162); Singapore Maritime Institute under the research project Grant (No. SMI-2015-OF-10); Natural Science Foundation of Fujian Province of China under Grant (No. 2017J05106); and Collaborative Innovation Center of High-End Equipment Manufacturing in Fujian.

Author contributions

R Zhou and M H Hong proposed the original idea and supervised the project. S D Lin and Y Ding fabricated the samples. H Yang and Y K K Ong performed the measurements. All authors commented on the manuscript.

Competing interests

The authors declare no competing financial interests.

Supplementary information

Supplementary information is available for this paper at https://doi.org/10.29026/oea.2018.180014